communications earth & environment

ARTICLE

https://doi.org/10.1038/s43247-022-00672-7 OPEN

Mangrove forests can be an effective coastal defence in the Pearl River Delta, China

Michela De Dominicis [1✉], Judith Wolf [1], Rosanna van Hespen [2,3], Peng Zheng [4,5] & Zhan Hu [6,7,8✉]

Coastal vegetation can reduce extreme water levels during storm events, but the controlling factors and processes in complex estuary or delta systems are still unclear. This limits an effective implementation of nature-based coastal defences in delta mega-cities in low-lying coastal areas. Here we have numerically modelled how mangroves can offer coastal protection to the large coastal cities located in the Pearl River Delta (China), such as Guangzhou and Shenzhen, during strong typhoons, like Hato (2017). Water level attenuation by mangroves is effective during extreme water level conditions and differences in mangrove forests' properties drive their coastal protection function. The local (within-wetland) attenuation of extreme water levels is more effective with wide vegetation patches and higher vegetation drag. Narrower vegetation patches can still provide non-local (upstream) water level attenuation if located in the upper estuary channels, but their design needs to avoid amplification of water levels in other delta areas.

[1] National Oceanography Centre, Liverpool, UK. [2] Department of Estuarine and Delta Systems, NIOZ Yerseke, Royal Netherlands Institute for Sea Research, Yerseke, The Netherlands. [3] Department of Physical Geography, Faculty of Geosciences, Utrecht University, Utrecht, The Netherlands. [4] Tianjin research institute for water transport engineering, Ministry of Transport, Tianjin, China. [5] School of Engineering, University of Liverpool, Liverpool, UK. [6] School of Marine Sciences, Sun Yat-Sen University, and Southern Marine Science and Engineering Guangdong Laboratory (Zhuhai), Zhuhai, China. [7] Guangdong Provincial Key Laboratory of Marine Resources and Coastal Engineering, Guangzhou, China. [8] Pearl River Estuary Marine Ecosystem Research Station, Ministry of Education, Zhuhai, China. ✉email: micdom@noc.ac.uk; huzh9@mail.sysu.edu.cn

Nature-based solutions refer to the aim to work with nature for tackling socio-environmental challenges, such as climate change, food and water security or natural disasters. Among those, the coastal protection benefits of natural ecosystems, often referred to as nature-based coastal defences, are increasingly being recognised within international and national coastal adaptation, resilience and sustainable development plans and strategies[1]. Based on the latest Nationally Determined Contributions submitted to the United Nations Framework Convention on Climate Change, a few coastal nations already explicitly advocate nature-based solutions for coastal protection, as a means to address future coastal hazards and sea level rise threats, with mangrove restoration as a common adaptation measure to enhance the resilience of local communities to climate change[2].

Mangroves are inter-tidal wetlands found along coastlines in much of the tropical, subtropical and warm-temperate world, where they naturally serve as the first line of defence against flooding and erosion. If existing mangroves were lost, 15 million more people would be flooded annually across the world[3]. Mangrove wetland restoration projects are starting to be widespread in several countries[4] for preserving their natural habitat and carbon sink function[5]. Understanding their value for coastal defence is also crucial for further encouraging their conservation and restoration. For cities located in estuaries or deltas, like many large Asian cities, the creation or restoration of mangrove wetlands between the city and sea could mitigate waves and the landward propagation of storm surges[6].

Wave height reduction due to the interaction with coastal salt marshes[7] and mangroves[8–13] is well established in the literature and mostly acts at the local scale of the wetland. Less well understood are the factors that control storm surge reduction by vegetation[14], with the majority of observational and modelling studies focusing on storm surge mitigation due to the resistance exerted by salt marshes[15–24] and few studies demonstrating the value of mangroves[25–31].

The effectiveness of the vegetation in dissipating storm surge and inundation is dependent on the density, height, width and fragmentation of the vegetation zones[15–19,23,27,29,30], as well as on intensity, duration, forward speed and track of the storm[15–17,20,22,24,27,28] and the surrounding case-specific larger-scale landscape settings[15,17,18,20–22,24,27,28,30]. The landward attenuation of the additional water level due to storms, referred to as within-wetland surge attenuation, is usually quantified as the rate of vertical reduction in storm surge height per horizontal inland distance over the wetland, ranging from 1.7 to 25 cm per km across salt marsh vegetation[14], with higher rates, 18–50 cm per km, across a mangrove forest[27,31].

The majority of studies investigating the effectiveness of vegetation for storm surge attenuation tend to address local (within-wetland) effects[14], while only few studies[18,24] investigated the non-local effects of coastal wetlands in complex estuary environments. Those studies have focused on salt marshes in estuaries in the Netherlands, Belgium and in the United Kingdom (UK) and examined the upstream surge attenuation, which is the contribution of wetlands to the reduction of surges that propagate upstream along an estuary. There is a lack of similar studies addressing the effects of mangrove forests at an estuarine-wide scale. A better understanding of how nature-based coastal defences, and in particular mangroves, interact within estuaries and complex deltas would help to boost the large-scale implementation of nature-based coastal defences, which at present is limited to a few projects in the UK and Belgium[6,18] involving the conversion of reclaimed land back to natural coastal wetlands.

Since mangroves cannot fully block the water, they are often combined with traditional flood defence structures like levees or seawalls. Mangrove forests placed in front of coastal protection structures reduce the risk of overtopping and direct wave impact[32], allowing for lower structures and, consequently lower construction costs. In the absence of levees or seawalls, mangrove forests may still reduce the extent of flooding, whereas even a small reduction in water level could already greatly reduce the extent of flooding in the low-lying areas behind the mangroves[33]. As the attenuation of storm surges increases with the width of the mangrove patch, wider mangrove forests could offer better protection for those low-lying areas, provided that enough accommodation space is available[34].

In this study, we investigate how coastal mangrove wetlands can modify the hydrodynamics of a complex delta coastal plain during extreme events, at both the local wetland scales and, more broadly, at the delta scales. The study focuses on the Pearl River Delta (Fig. 1a, b), a site containing complex river systems, with several bifurcating and coalescing river branches, where water levels are influenced by the interaction of the river runoff, tides and storm surges from the South China Sea. The Pearl River Delta flood plain is also home to several very large cities ('mega-cities'), including Hong Kong, Shenzhen and Guangzhou (Fig. 1b), that are experiencing an exponential population and economic growth, and thus an expansion of areas vulnerable to coastal flooding[35].

Estuarine mangroves within the broader Guangdong—Hong Kong—Macao Greater Bay Area, where the Pearl River Delta is located, have first undergone a loss and then a gain of the area over the last 30 years. Nearly 40% of mangrove areas were lost during the 1990s, mainly resulting from human exploitation of the coastal landscape (conversion to built-up area and aquaculture ponds), but from 2000 to 2018, the mangrove area has increased thanks to the establishment of nature reserves[36]. In the Pearl River Delta only, a net loss of 11.73 km^2 (45%) of mangroves during the period between 1985–2015 has been detected in the analysis of satellite imagery[37]. While these studies demonstrate the dramatic reduction in mangrove extent and subsequent degradation of the ecological function of these habitats, the previous range indicates that the coastal areas investigated are suitable mangrove habitats. Thus re-vegetation of coastal areas by mangroves is a potentially viable ecosystem-based coastal adaptation measure. The remaining few small patches of mangroves in the Pearl River Delta are found in the lower estuary, along the coast of Qiao Island, Shenzhen Bay and Lingding Bay[36] and in the upper estuary close to Guangzhou, along the river channels of the Nansha and the Panyu district[38]. Guangzhou is crossed by several urban channels, most of which directly connect to the South China Sea, increasing the city's exposure to coastal flood risks. Guangzhou has been identified as the most vulnerable city in the world in terms of annual economic losses due to flooding[39]. Shenzhen is presently ranked as the ninth most vulnerable city to sea level rise, but it is projected to rise to the fourth most vulnerable by 2050[39]. The vulnerability of these two cities to coastal hazards motivated the present modelling investigations. In this study, we numerically modelled the protection capability of the mangrove wetlands in Shenzhen Bay (Fig. 1c) and in the upper estuary river branches close to Guangzhou (Fig. 1d) to determine their ability to mitigate coastal flooding. In Shenzhen Bay, the presence of mangroves located in two natural reserves (Futian Nature Reserve and Mai Poi Nature Reserve), where mangrove conservation and restoration effort have been conducted[36], was simulated (Fig. 1c). The Shenzhen Municipal Government has also initiated a large coastal reclamation project for some areas in the Futian coastal wetland[35], which could interact and alter its function as flood-storage area. For the upper delta location, we simulated two hypothetical mangrove forests, which are an expansion of the existing small mangrove plantations located in

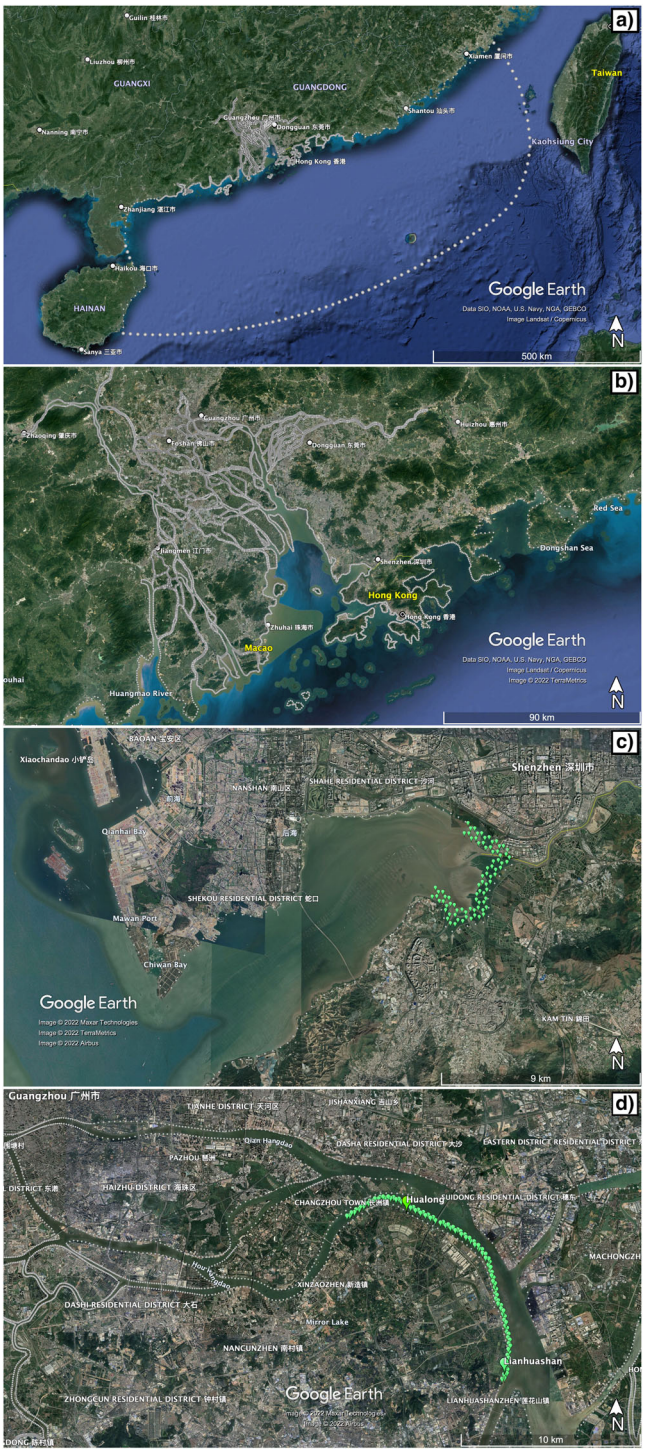

Fig. 1 Google Earth view of the Pearl River Delta and South China Sea and FVCOM model domain. Open boundary and the coastal nodes of the FVCOM model grid are indicated by the grey dots in (**a**); a close-up of the model grid with the location of main cities, like Shenzhen and Guangzhou, in (**b**); a close-up of Shenzhen Bay in (**c**) and a close-up of the river channels close to Guangzhou in (**d**), with the location of the model elements belonging to the modelled mangroves patches (green placemarks).

one of the river channels just downstream of Guangzhou (Fig. 1d). To explore the effects of vegetation on storm surge dynamics and currents, we used a Finite Volume Community Ocean Model (FVCOM) implementation for the South China Sea and the Pearl River Delta (model domain in Fig. 1a and model bathymetry in Fig. 2a, c) and simulated Typhoon Hato (2017) one of the strongest typhoons to affect the coastal areas of the Pearl River Delta in recent decades[40]. Additionally, we analyzed how the effectiveness of mangroves changes under different sea level rise (SLR) scenarios.

In this work, we show that water level attenuation by mangroves varies in space and in time and cannot be summarised into a single linear reduction factor. The vegetation properties and the location of the mangroves within the delta play an important role. In general, if mangroves are located in open bays and open coastlines they will affect the water levels mostly locally (within-wetland), instead if located in the delta river channels, they will also influence non-local water levels (upstream water level attenuation). Both within-wetland and upstream attenuation are at their highest during extreme water levels, like those experienced during strong typhoons.

Results

The level of protection offered by a vegetation patch located in the natural reserves in Shenzhen Bay with a width of 600 m, which is about the width of the vegetation patch actually present, is shown in Fig. 3. The same figure demonstrates the loss in protection if the mangroves decrease in size to 300 m or disappear completely, as well as the changes in protection with a wider mangrove forest (900 m) (see Fig. 2b). Figure 3 analyses the total, tide and surge water levels along the coast, with and without the mangroves, for 24 h, spanning before and after the water level peaks driven by Typhoon Hato. The temporal trends represent the average value among all the mangrove patch coastal nodes (blue squares in Fig. 2b). Each experiment is performed twice (see Experiments 01–06 in Table 1): fully forced (panel a) and tide-only (panel b). Tide and surge contribute to the total water level. The surge is calculated as the difference in water levels between the tide-only and the fully forced runs (panel c). We refer hereafter as 'high-drag vegetation' to the experiments (see a full description of experiments in the section 'Method') with drag coefficient $C_D = 4$ and flow-facing area per tree $A = 3\ m^2$ (mangroves with leaves), and as 'low-drag vegetation' to those with $C_D = 2$ and $A = 1\ m^2$ (mangroves without leaves). The drag coefficient and flow-facing area depend on the mangrove species, age and presence/absence of leaves.

The maximum total water level at the coast (on 23 August 2017 at 06:00 UTC (Coordinated Universal Time), the time Typhoon Hato passed closest to the Pearl River Delta) is overall reduced from 3.3 to 2.1 m by the vegetation patch of 600 m (the width of the vegetation patch actually present) when a high-drag vegetation is applied (green solid line in Fig. 3a). A 600 m patch with a low-drag vegetation and a narrower vegetation patch (300 m) with high-drag vegetation (dashed green and light green lines in Fig. 3a) are effective in reducing the total water level in the hours before reaching the peak, but not in reducing the peak itself. A wider vegetation patch (900 m) with high-drag vegetation would instead greatly reduce the total water level, which then reaches only 0.5 m at the coast (orange solid line in Fig. 3a); the same width but low-drag vegetation leads instead to a reduction of 0.8 m at the coast (dashed orange line in Fig. 3a).

The maximum tidal elevation (on 23 August 2017 at 03:00 UTC) is changed only by the 900 m vegetation patch with high-drag vegetation, showing a 0.1 m decrease in the maximum tidal height (orange solid line in Fig. 3b). However, the tides are delayed in all experiments. This time delay becomes more evident with high-drag vegetation 600 and 900 m patches: half hour delay and 1 h delay, respectively (Fig. 3b). This shift leads to an apparent increase (of about 0.1–0.3 m) in tidal elevation when the

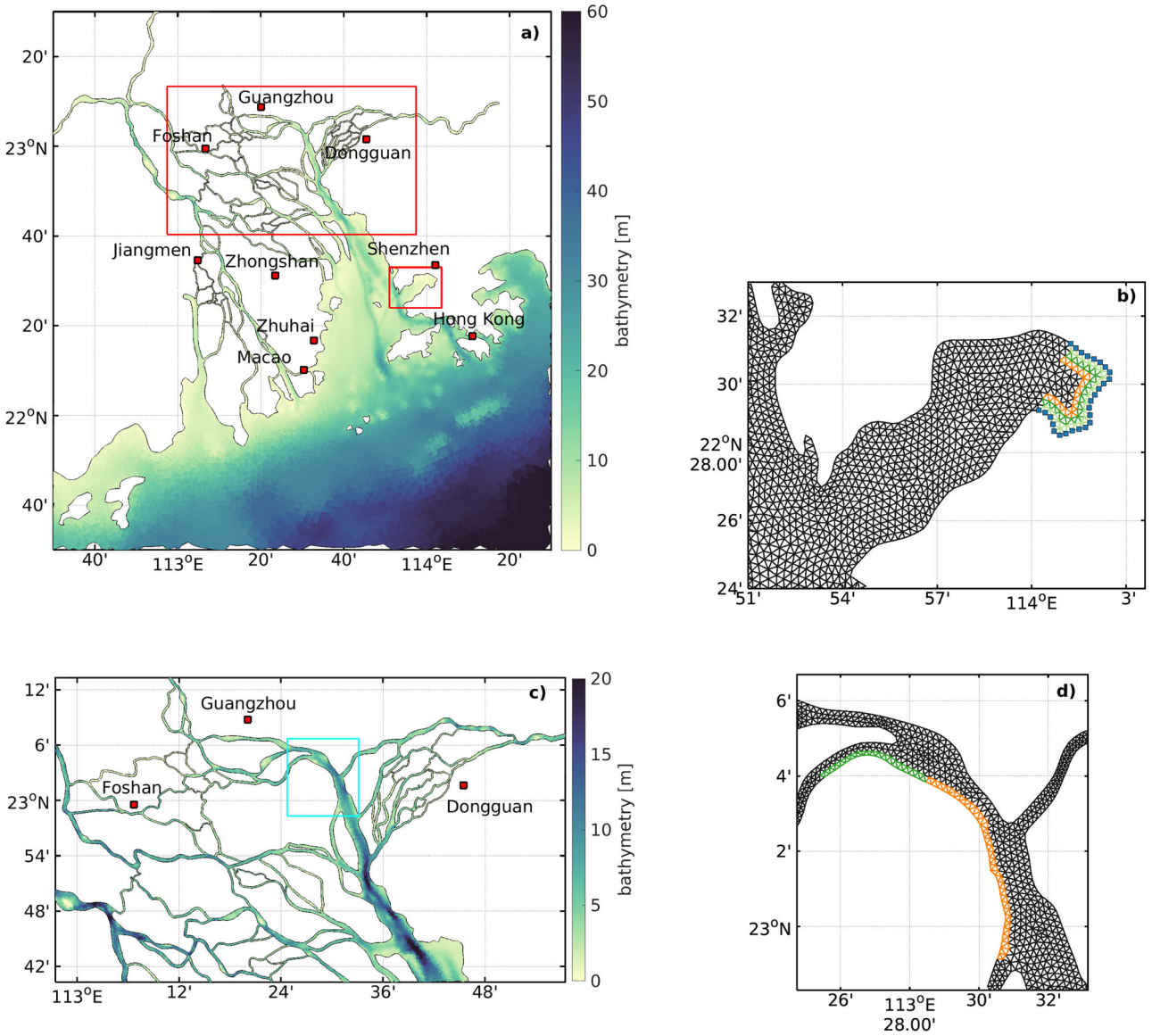

Fig. 2 FVCOM model bathymetry and grid. Bathymetry within the Pearl River Delta and adjacent South China Sea (**a**), the boxed regions highlighted in red are the areas of Shenzhen Bay shown in (**b**) and the upper river channels where Guangzhou is located shown in (**c**). Close-up view of the FVCOM model grid in Shenzhen Bay (**b**), model elements coloured light green indicate the theoretical 300 m mangrove extent, dark green indicates the present 600 m extent, and orange indicates the theoretical 900 m extents, blue squares are the mangrove patch coastal nodes. Close-up view of the bathymetry within the upper channels (**c**), the boxed region highlighted in light blue is the region shown in (**d**). Close-up view of the model grid from Hualong to Lianhuashan (**d**), model elements in green are the small patch close to Hualong and orange elements are the extension up to Lianhuashan.

tide is falling, which contributes in reducing further the surge when the total water level peaks (surge is calculated as the difference between total water level and tidal elevation, thus if the tidal elevation increases the surge decreases).

The maximum surge level (on 23 August 2017 at 06:00 UTC) along the coast is halved (from 2.8 to 1.4 m) by the 600 m vegetation patch with high-drag vegetation (green solid line in Fig. 3c). As observed for the total water level, there is an apparent big surge reduction before reaching the peak with the low-drag vegetation 600 m and high-drag vegetation 300 m patches (dashed and light green lines in Fig. 3c), however when reaching the peak the surge at the coast is not reduced or only slightly reduced (5 cm). This can be explained as a delay of the currents bringing water from the open ocean toward the coast, pushed toward the shore by the force of the wind, similar to the delay observed for the tides. A wider vegetation patch (900 m) with high-drag vegetation leads instead to a total suppression of the surge at the coast (−0.3 m) (orange solid line in Fig. 3c), the same width but low-drag vegetation leads instead to a reduction of 1 m (dashed orange line in Fig. 3c).

Before the passage of Typhoon Hato (before 23 August 2017 04:00 UTC), the total water level and the surge both increased when vegetation is present in the model, 0.3 m for the total water level and 0.6 m for the surge (for the high-drag vegetation 600 m patch). The time delay in tides leads to an apparent decrease/increase in tides of about 0.3–0.5 m, that could affect the water depth and have consequences on the surge. However, an increase in the surge before the peak has been observed in a run without tides too (see Supplementary Fig. S.1), this means it cannot be fully attributed to the changes in the tidal modulation of the surge.

The surge reduction offered by mangroves changes under different SLR scenarios. Figure 4 shows how the effectiveness of the high-drag vegetation 600 m patch changes under three SLR

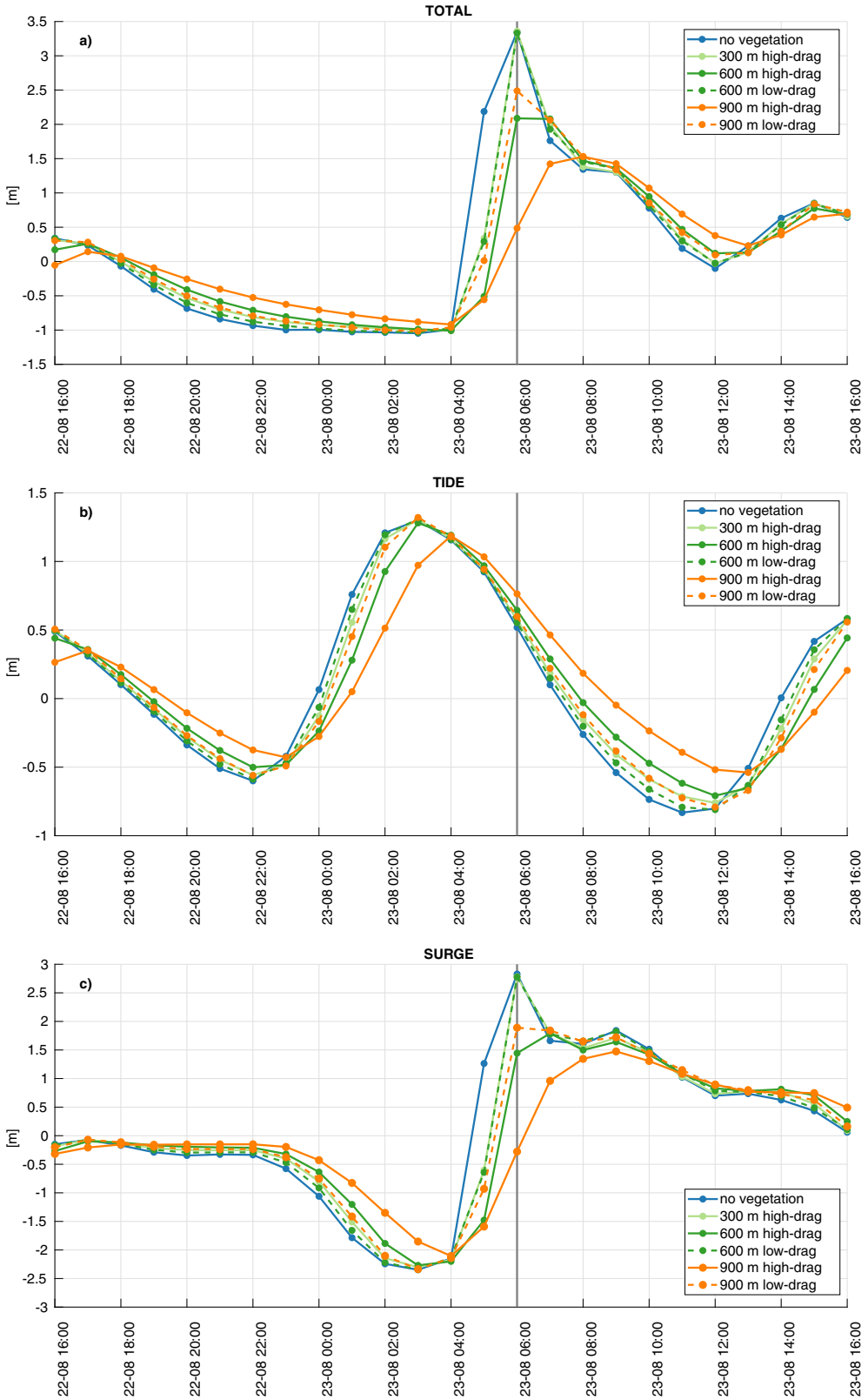

Fig. 3 Water levels with and without vegetation in Shenzhen Bay during Typhoon Hato. Total water level (**a**), tide-only (**b**) and surge only (**c**) with and without vegetation in Shenzhen Bay. The temporal trends represent the average value among all the mangrove patch coastal nodes (blue squares in Fig. 2b). The grey vertical line indicates the time Typhoon Hato passed closest to the Pearl River Delta. Times are in UTC.

Table 1 Sensitivity experiments to mangrove patch location, width and vegetation properties during Typhoon Hato.

Experiment[a]	Location	Patch width	Drag coeff.	Max. project. area	SLR
01[b]	-	-	-	-	0 cm
02	Shenzhen Bay	300 m	4	3 m^2	0 cm
03[b]	Shenzhen Bay	600 m	4	3 m^2	0 cm
04	Shenzhen Bay	600 m	2	1 m^2	0 cm
05	Shenzhen Bay	900 m	4	3 m^2	0 cm
06	Shenzhen Bay	900 m	2	1 m^2	0 cm
07	Hualong	300 m	4	3 m^2	0 cm
08	Hualong-Lianhuashan	300 m	4	3 m^2	0 cm
09	Hualong	300 m	2	1 m^2	0 cm
10	Hualong-Lianhuashan	300 m	2	1 m^2	0 cm
11	-	-	-	-	30 cm
12	-	-	-	-	50 cm
13	-	-	-	-	90 cm
14	Shenzhen Bay	600 m	4	3 m^2	30 cm
15	Shenzhen Bay	600 m	4	3 m^2	50 cm
16	Shenzhen Bay	600 m	4	3 m^2	90 cm
17	Hualong-Lianhuashan	300 m	4	3 m^2	30 cm
18	Hualong-Lianhuashan	300 m	4	3 m^2	50 cm
19	Hualong-Lianhuashan	300 m	4	3 m^2	90 cm

[a]Each experiment is performed twice: tide-only and fully forced. The surge is the difference in water levels between the tide-only and the fully forced runs.
[b]Experiment 01 and 03 have also been performed with atmospheric forcing only, to exclude tidal modulation on the surge.

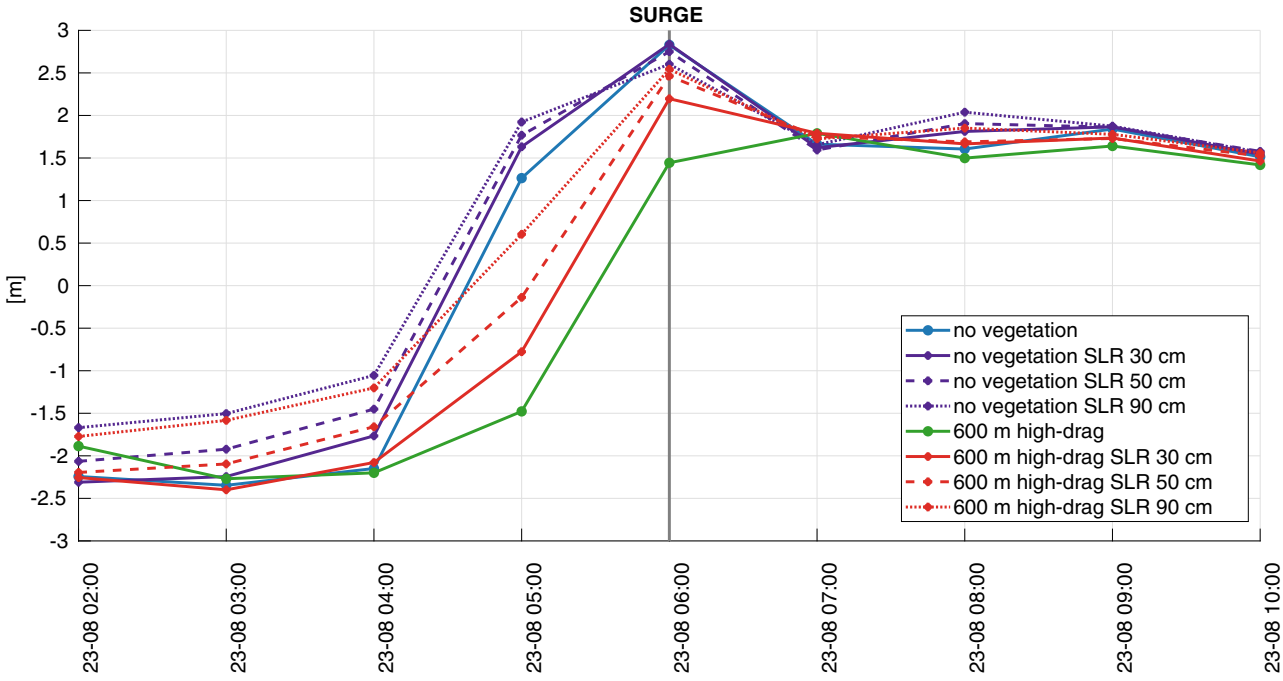

Fig. 4 Surge levels with and without vegetation in Shenzhen Bay under different SLR scenarios. Surge levels with and without a high-drag 600 m vegetation patch in Shenzhen Bay under different SLR scenarios (30, 50, 90 cm). The temporal trends represent the average value among all the mangrove patch coastal nodes (blue squares in Fig. 2b). The grey vertical line indicates the time Typhoon Hato passed closest to the Pearl River Delta. Times are in UTC.

scenarios (30, 50, and 90 cm). With 30 cm SLR, the vegetation will reduce the surge, however, the surge will reach 2.2 m, which is higher than what was simulated without SLR. The mangroves will be even less effective with 50 cm SLR and 90 cm SLR, when the surge will reach roughly 2.5 m (dashed and dotted red lines in Fig. 4). The friction of mangroves will be less effective in dissipating the surge with SLR due to the vegetation being placed in a deeper water column. This is because in the model simulations, we are assuming the coastline is fully protected and mangroves are placed in front of a seawall and no extra land gets inundated. At the same time, under the different SLR scenarios, the surge will also decrease with SLR (purple lines in Fig. 4). This is due to the wind stress being less effective in pushing a deeper water column, leading to a reduction of the maximum surge during extreme events[41]. This means that with 90 cm SLR, the surge reduction due to mangroves is nearly zero (dotted red line and dotted purple line in Fig. 4), although there is a reduction in the hours before the peak is reached.

Figure 5 shows how the surge (a–d) and current speed (e–h) change during extreme water level conditions in Shenzhen Bay (from 04:00 to 07:00 on 23 August 2017) due to the presence of the high-drag vegetation 600 m patch (Experiment 03 in Table 1).

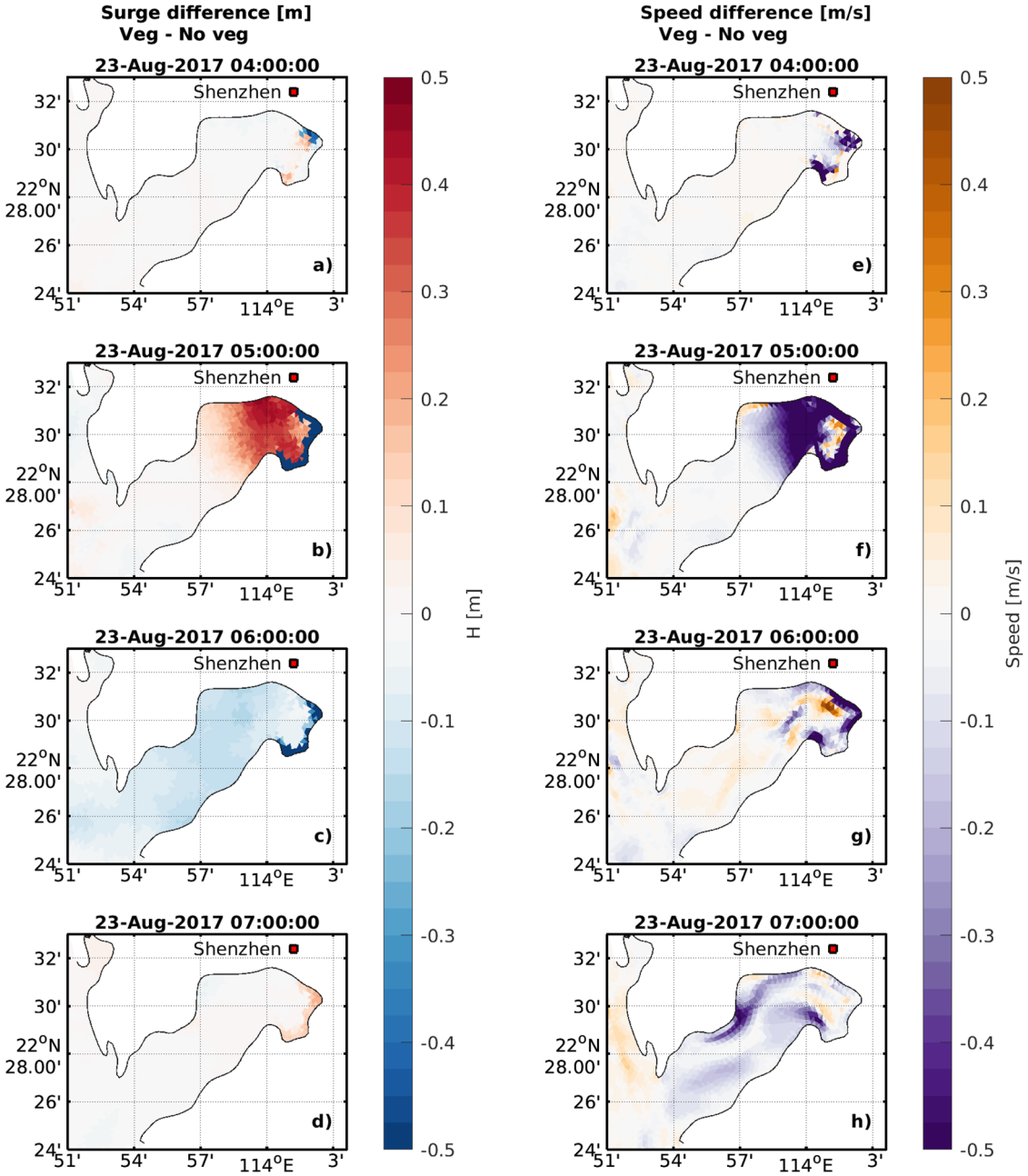

Fig. 5 Surge and current speed spatial changes due to vegetation in Shenzhen Bay during Typhoon Hato. Surge (**a**–**d**) and current speed (**e**–**h**) spatial changes in Shenzhen Bay due to the 600 m high-drag vegetation patch during extreme water level conditions from 04:00 to 07:00 on 23 August 2017 (Experiment 03 in Table 1). Blue/Red (purple/orange) means a decrease/increase due to the presence of vegetation. Times are in UTC.

The other experiments show similar patterns but lower values (Experiments 02 and 04, see Supplementary Figs. S.2, S.3) or more intensity of changes (Experiments 05 and 06, see Supplementary Figs. S.4, S.5). One hour before the total water level peaks along the coast of Shenzhen Bay (on the 23 August 2017 at 05:00 UTC), there is a decrease of the surge in the vegetation patch and an increase in the surge in the rest of the bay. This pattern is connected to a decrease in the current speed in the vegetation patch, which is driven by the local vegetation friction, and a decrease in speed in the bay in the same location where the surge increases. When the water travelling from the open ocean into the bay, pushed toward the shore by the force of the wind, feels the friction of the vegetation, this causes a decrease in the speed of the currents bringing water toward the coast (i.e. slow down of the surge propagation speed) and consequently a temporary increase in a surge in the middle of the bay (i.e water piling up in the bay). When all the water pushed by the force of the winds reaches the shore on 23 August 2017 at 06:00 UTC, the changes are a local (in the vegetation patch) decrease in surge and current speed due to the vegetation friction. The vegetation effect of decreasing the current speed in such extreme events is relevant for reducing erosion along the coast, while local increases in current speed are visible outside of the vegetation patch.

The Shenzhen Bay mangrove forest experiments have shown that mangroves can locally attenuate the surge travelling over the vegetation towards the shoreline. In estuaries, upstream surge attenuation, i.e. the cumulative surge reduction over large distances along confined estuary channels, is also likely to mitigate extreme water levels in vulnerable upper delta regions, like the Guangzhou area. Here, we show how hypothetical mangrove

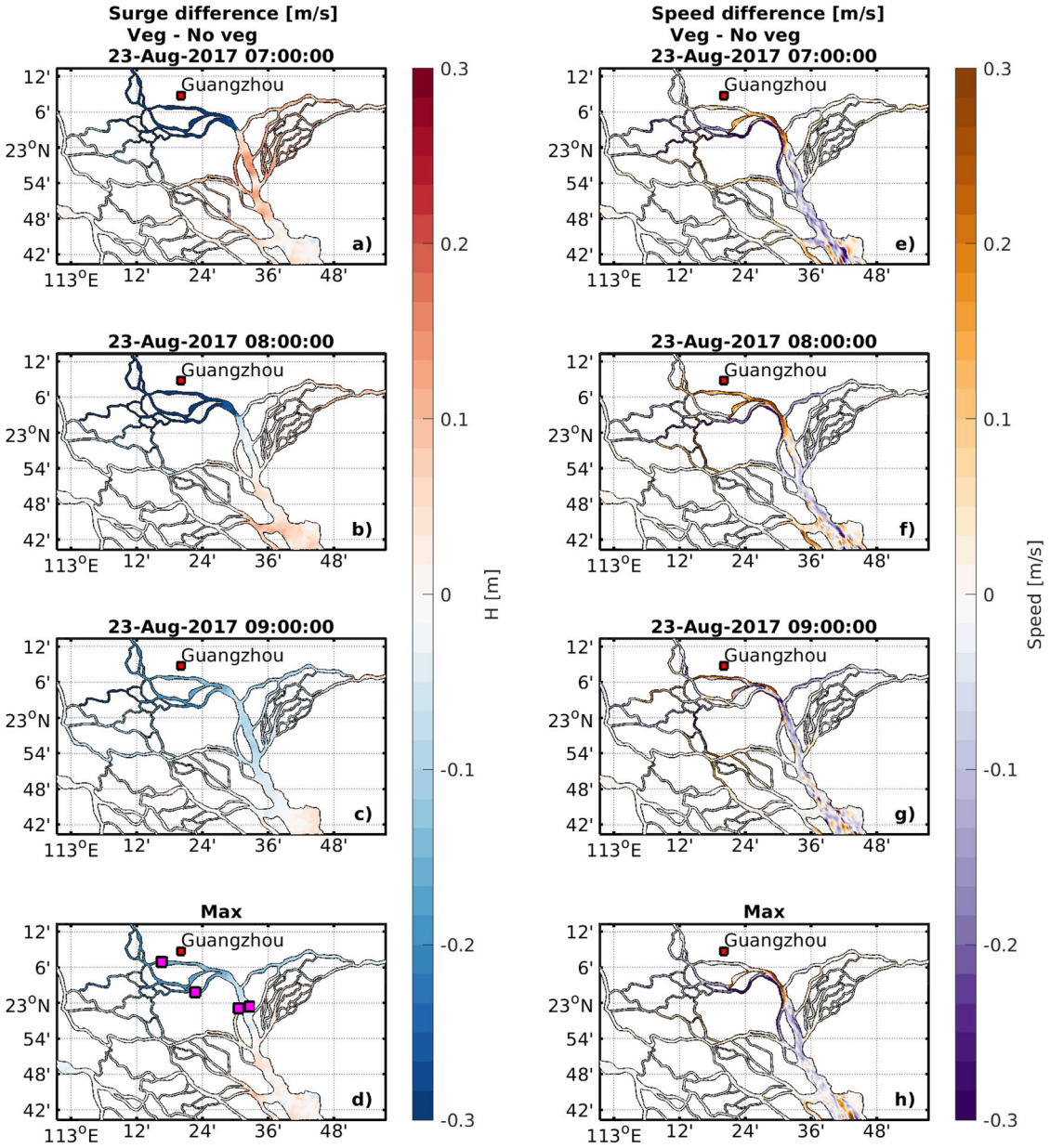

Fig. 6 Surge and current speed spatial changes due to vegetation in the upper estuary river channels close to Guangzhou during Typhoon Hato. Surge (**a**–**c**) and current speed (**e**–**g**) spatial changes in the upper estuary due to the 300 m high-drag vegetation patch extending from Hualong to Lianhuashan (Experiments 08 of Table 1) between 07:00 and 09:00 on 23 August 2017 and difference in the maximum surge (**d**) and current speed (**h**) at any time. Blue/Red (purple/orange) means a decrease/increase due to the presence of vegetation. Pink squares in (**d**) are the starting and end points of the coastline sections used in Fig. 7. Times are in UTC.

forests, located in the river channels in the upper delta areas (Fig. 2c), change the water levels upstream, where Guangzhou is located. We show here the results with different patch lengths (see Fig. 2d) and vegetation drag coefficients (we did not test varying patch width because the channels are too narrow to accommodate mangrove forests wider than 300 m). The effect of vegetation is maximum just before and when the surge peaks in the area, between 07:00 and 09:00 on 23 August 2017. Figure 6 shows the effect of the 16 km patch from Hualong to Lianhuashan (Experiment 08 in Table 1). Cumulative mangrove drag first delays and then overall reduces the surge level in the upstream delta channels close to Guangzhou, at the same time, the vegetation patch (Fig. 6a, b) amplifies the surge level downstream of the mangrove forest (towards the estuary mouth) and in the eastern river channels, as the surge is less able to propagate upstream of the mangrove forest (blockage effect). The vegetation patch has the largest blockage effect when the surge is reaching the area between 07:00 and 08:00 on 23 August 2017, acting as a solid obstacle rather than dissipating energy, diverting some water into the eastern channels and increasing the water level downstream of the vegetation patch (Fig. 6a, b). This downstream water level increase is dissipated when the surge has peaked in the area (Fig. 6c), and as a consequence, the blockage effect is reduced too. While the large surge reduction (>0.3 m), visible at 07:00 and 08:00 on 23 August 2017 (Fig. 6a, b), can be attributed to a delay (induced by the vegetation) of the surge travelling up in the estuary, when the surge peaks in the area at 09:00 on the 23 August 2017 (Fig. 6c), the cumulative mangrove drag overall reduces the surge level upstream. The change in the maximum surge at any time (Fig. 6d) is a more meaningful measure, i.e. not

affected by shifts in time, to understand how effective, or disruptive, the vegetation is. It shows indeed, a surge reduction exceeding 0.2 m in the upstream delta channels close to Guangzhou, while the increase in the eastern river channels is nearly negligible.

Current speed (Fig. 6e–h) is decreased locally in the vegetation patch and in one of the river branches, likely reducing erosion along the coast. However, it is increased in the river branch further upstream where Guangzhou is located, thus likely increasing erosion there. The spatial changes in surge and current speed induced by the low-drag vegetation long patch (Experiment 10 in Table 1) and the high- and low-drag vegetation short patch (6 km, Hualong) are not shown here (Experiments 07 and 09 in Table 1), they have a similar pattern but less intensity than the high-drag vegetation long patch (see Supplementary Figs. S.6–S.8).

Figure 7 shows how the 300 m high-drag and low-drag vegetation patches of different lengths (6 and 16 km) change the

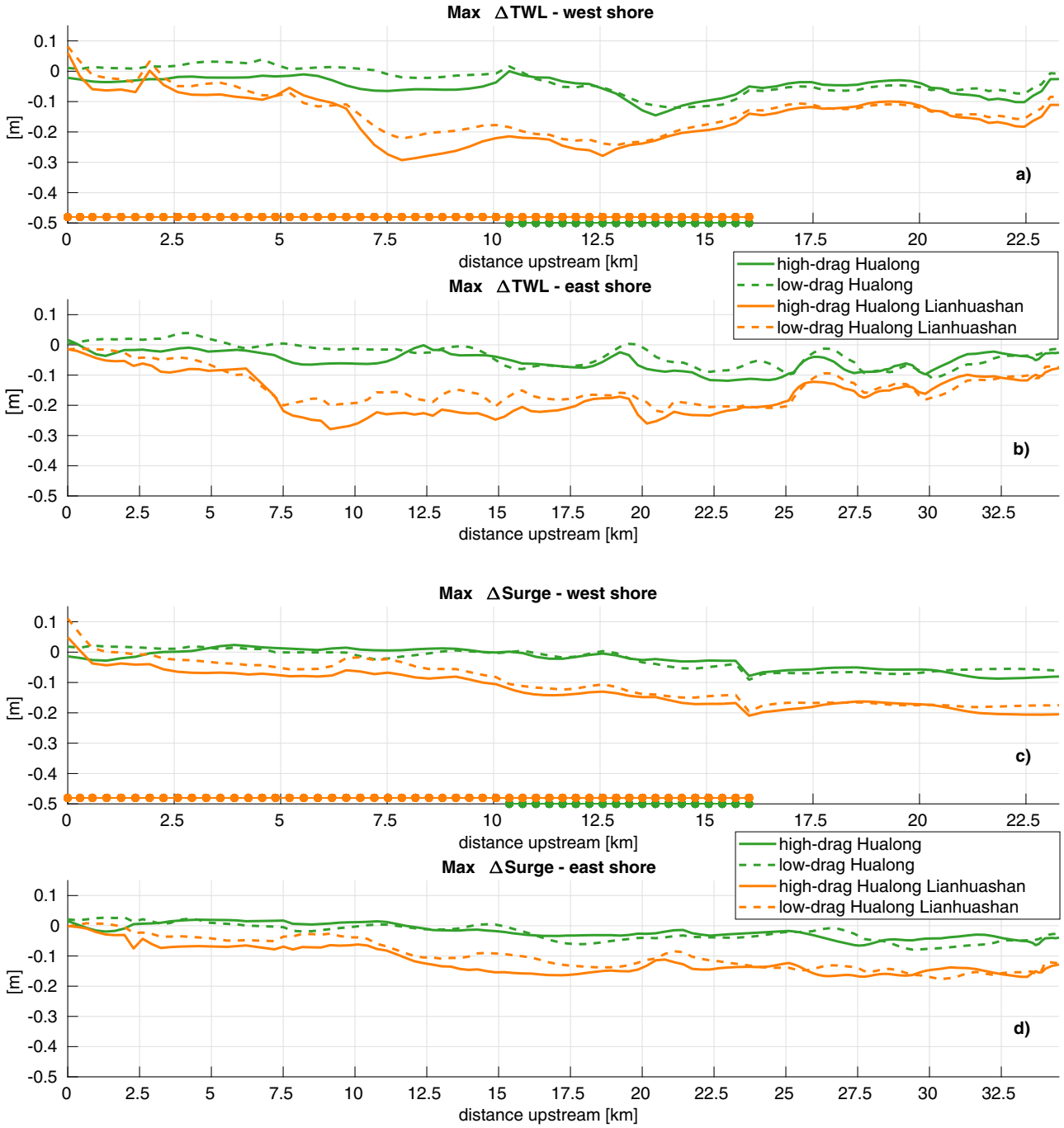

Fig. 7 Change in the maximum total water level and surge due to vegetation in the river channels close to Guangzhou during Typhoon Hato. Change in the maximum total water level (TWL) and surge at any time (during the passage of Typhoon Hato) compared to the no vegetation scenario due to the 300 m high-drag and low-drag long and short vegetation patches extending from Hualong to Lianhuashan (Experiments 07,08,09,10 of Table 1), from the southernmost edge of the mangrove patch and going upstream along the west shore (**a**, **c**) and along the east shore up to the channel where Guangzhou is located (**b**, **d**). The bottom circles identify where the patches are located along the coastal sections (green—Hualong; orange—Hualong to Lianhuashan). Times are in UTC.

maximum total water level and surge at any time during the passage of Typhoon Hato, starting from the southernmost edge of the mangrove patch and going upstream along the west shore (Fig. 7a, c) and along the east shore up to the channel where Guangzhou is located (Fig. 7b, d) (start and end points of the coastal sections are the pink squares in Fig. 6d). The maximum total water level and surge are reduced by the cumulative drag of the mangrove forest. The reduction gets larger going upstream in the vegetation patch (the location of the mangrove patch along the coastal section is identified by green and orange circles in Fig. 7a, c) and it is sustained further upstream outside of the vegetation patch. The largest reductions in total water level (0.3 m) and surge (0.2 m) are achieved with the high-drag vegetation longest patch, along the west shore (Fig. 7a, c), where the mangrove forest is actually located. Along the east shore of the upstream river channel where Guangzhou is located, the maximum reduction is obtained with the high-drag vegetation longest patch and it is 0.2–0.3 m for the total water level and 0.1–0.2 m for the surge. With the shorter vegetation patch the maximum reduction, in both total water level and surge, is <0.1 m along both the west and east shore. For both the long and short patches the high-drag vegetation patch is slightly more effective than the low-drag vegetation patch.

We have analyzed how the effectiveness of the high-drag vegetation patch from Hualong to Lianhuashan change under different SLR scenarios (30, 50 and 90 cm), and we found the vegetation will be still able to reduce the total water level in the upstream river channels where Guangzhou is located, with similar spatial changes as the ones simulated with no SLR (see Supplementary Fig. S.9). Differently from the Shenzhen Bay mangrove patch experiments, where the mean total water level uniformly increases by the SLR amount, in the upstream river channels SLR will interact with the river discharge and tides in a complex way. As described in a previous study[41], SLR will not increase the total water level by the same amount everywhere in the Pearl River Delta. The western river channels will be influenced by the interaction of SLR, river discharge and tides. While tides will see an amplification due to SLR-induced depth changes and consequently reduced bottom friction, the river discharge will halve the increase in mean water level due to SLR.

Discussion

The Pearl River Delta is a coastal region with a large population, projected to be more than 120 million people by 2050, that has become a global economic hub, dominated by the manufacturing, logistic, tourism and finance industries[35]. Traditional hard-engineered flood protection measures remain a favourite option, but less than 4% of Guangzhou is protected to at least the 1-in-100-year flood frequency and most flood-prone areas are protected only for the 1-in-20-year flood frequency or below[35]. The current urbanisation and industrialisation rate means also that more areas are becoming vulnerable to flooding and need to be protected. Flood defences by hard-engineered approaches alone are, therefore, unlikely to be economically sustainable under current rates of climate change and urban expansion. Nature-based coastal defences could be used in conjunction with hard-engineered defences to reduce their cost[42]. To the contrary, in some areas of the Pearl River Delta, land reclamation has extended the coastline 1 km seawards in the last decade, and most reclaimed land has been converted from mangrove coastal wetlands[35,36], which originally acted as a buffer to extreme water level.

In 2017, the State Forestry Administration of China released a 10-year plan called 'The Planning of Establishing National Coastal Shelter Forests' (2016–2025), in which the 'Mangrove Forest Restoration Project' is listed as a key project[43]. The local (behind the wetland) protection offered by nature-based coastal defences has been demonstrated[14]. However, large-scale implementation of mangrove restoration for coastal protection, in a physically complex area like the Pearl River Delta, with major outlets of three main tributaries of the Pearl River and several river branches connected with the South China Sea, requires a full understanding of the local and non-local effects of vegetation in a deltaic area. The latter can be achieved with location-specific modelling of the complex deltas dynamics and their interactions with mangroves, as we did in the present study for the Pearl River Delta. The obtained knowledge is of value to the management of the spatial planning of mangrove-based coastal defence in the Pearl River Delta. Similar studies are necessary for the real-life implementation of nature-based coastal defences in other urban deltas worldwide.

In Shenzhen Bay, where mangroves are present, they attenuate the water level during extreme water conditions, while a slight amplification is observed during calm conditions, however, flood risks are not exacerbated since amplification rates are very small. The local, within-wetland, attenuation of extreme water level (total) can vary from 0 to 2.8 m, depending on the width of the patch and the mangrove forest properties. Hypothetical 300 m wide mangrove forests located in the upper estuary (where some mangrove plantations exist) contribute to the reduction of surges that propagate upstream where Guangzhou is located. Thus, narrow vegetation patches (up to 300 m) can be effective if located in estuarine/deltaic settings as they can provide upstream (total) water level attenuation, which in Guangzhou is about 0.1–0.3 m, depending on the length of the patch and the mangrove forest properties. Mangroves in the upper river channels can also create blockage effects, thus complex deltas need accurate modelling of specific interventions to understand which are the areas that can eventually see an amplification of water levels and under which conditions.

While empirical data and modelling studies are available for within-wetland surge attenuation by salt marshes[14], there are only a few observational studies about surge attenuation rates observed in mangrove forests[27,29] and none of them are in deltas, where some of the largest mangrove trees in the world are located. We found that a 600 m patch could provide a surge attenuation up to 1.4 m (233 cm per km) with the high-drag vegetation. These values are larger than the attenuation rates for salt marshes, showing that, to offer coastal protection, a narrower wetland is needed with mangroves compared to the width required with salt marshes (at least 10 km wide[14]). Our simulations are based on the drag coefficients of mangrove branches sampled in the Pearl Delta and measured in flume experiments[44]. A comparison with measurements in situ would be desirable to validate our results. However, the surge attenuation rates discussed in this study are during typhoon conditions, which are inherently rare events (and it is dangerous to collect data under such conditions), thus it is not surprising that no field data exist.

In this work, the upstream water level attenuation that we observed in Guangzhou is due only to cumulative vegetation drag and not to a water storage effect of additional inundated land, as in other studies[18], because it is not realistic in a highly urbanised region like the Pearl River Delta where the coastline and river shores are 'fixed', i.e. protected. A nature-based coastal defence scenario, where coastal societies retreat from the coast, is more likely in rural, sparsely-populated areas[45], where more space is available for accommodating an expansion of coastal wetlands. However, future-proofing schemes of urban areas could also opt for the accommodation of flood buffer areas depending on the specific settings and socio-economic circumstances.

Similarly, the SLR scenarios presented in the paper show what will happen with mangroves placed in front of a fully protected coastline. However, in the absence of seawalls and where inland areas are accessible and suitable for the establishment, mangroves could shift inland. Additionally, under the right circumstances, mangroves may respond to relative SLR by shifting vertically, if the accumulation of sediments (not modelled in this work) raises the forest floor at a pace similar to SLR[46].

In general, we found that the effective design of nature-based coastal defences requires location-specific realistic predictions to be done prior to extensive restoration efforts. This should be done in conjunction with an understanding of the survivability of mangroves in that specific setting. We keep this as a question for future studies to understand what the minimal level of surge reduction that would make an extensive restoration effort a successful investment for flood mitigation, which should also take into consideration other ecosystem services offered by mangroves, i.e. carbon storage, biodiversity, prevention of coastal erosion, fisheries, water quality.

Method

We used an FVCOM[47] implementation for the South China Sea and Pearl River Delta, with an unstructured grid that extends from a coarse grid (>10 km) in the open ocean to an appropriately high resolution (100 m) in the delta distributary channels, with 25 uniform σ (terrain following) vertical layers. The model has been previously validated and used to explore future interactions between sea level rise, tides and storm surges[41,48]. Water level time series have been validated against observed data from four coastal stations (root mean square error <20 cm) and average tidal range levels have been also validated using 23 tide gauges located in the river branches[41]. Comparison between the total water level modelled and observed at the Hong Kong tide gauge during typhoons Hato is also presented in a previous study[41].

To understand what is controlling the effectiveness of mangroves, we modelled several scenarios with different locations of mangroves (in Shenzhen Bay and in the upper estuary) and mangrove properties. In Shenzhen Bay, we have simulated a mangrove forest of 600 m, which is about the width of the vegetation patch actually present (Fig. 1c) and the loss in protection if the mangrove forest decreases in size to 300 m or disappears completely, as well as the changes in protection with a wider mangrove forest (900 m) (Table 1 and Fig. 2b). For the upper delta location, we have analyzed the level of protection which would be provided by two hypothetical mangrove forests of 300 m width and of different length. These hypothetical patches include some existing mangrove plantations: the short patch (6 km) includes the mangrove plantation in Hualong and the long patch (16 km) encompasses the Hualong and Lianhuashan mangrove plantations (Panyu District) (Figs. 1d, 2d). In the upper estuary, we did not test the sensitivity to the width of the mangrove patch because the channels are too narrow to accommodate mangrove patches wider than 300 m, and we did not test varying lengths in Shenzhen Bay because we wanted to reproduce the length of the mangrove patch that is actually present.

The resistance created by vegetation has been previously modelled by increasing the bottom friction[15,19,20,22–24,27,28,30]. A more accurate approach, used in this study, is to consider the vegetative drag within the water column using a momentum sink approach, i.e. adding an additional drag force in the three-dimensional momentum equation. This same approach has been used for modelling other underwater features, including kelp vegetation[49], tidal turbines[50,51], wind farm pylons[52] and aquaculture farms[53]. We do not consider any turbulence generation/dissipation induced by vegetation, as done in other studies[16,17,21]. The vegetation-induced resistance horizontal force, **F**, has been implemented in FVCOM as a quadratic drag law in the form[54]:

$$\mathbf{F} = -\frac{1}{2}\rho C_D A|\mathbf{u}|\mathbf{u}N \quad (1)$$

where ρ is the water density, C_D is the mangrove drag coefficient, $\mathbf{u}$ is the fluid velocity, A is the flow-facing area per mangrove tree and N is the number of mangrove plants in the model element. Since the mangroves can span multiple model vertical σ layers, a fraction of the resistance force (proportionally to the layer thickness) is exerted in each model layer occupied by the mangroves. To obtain an estimate of N we assumed a homogeneous dense mature tall forest with a mangrove density of 0.5 plant per m^2[55]. The drag properties for five different mangrove species sampled across several sites in the delta have been measured in flume experiments[44], with C_D ranging from 1.85 to 14.47 (with currents of 0.15 m s^{-1}) depending on the mangrove species and presence/absence of leaves. We are looking at both with/without leaves, because mangroves can lose leaves during a storm[56]. We chose to use the lower threshold of C_D values among the five species common in the Pearl River Delta: $C_D = 2$ for mangroves without leaves and $C_D = 4$ for mangroves with leaves (see description of experiments in Table 1). We use the same drag coefficients for both Shenzhen Bay and the upper delta locations, thus not considering the specific type of mangroves present (or possibly present) in each specific area. To calculate the projected frontal surface area per tree A, we considered a trunk diameter of about 10 cm, which is the average value for the Pearl River Delta species[44]. By assuming that trees grow like a fractal[57], where each subsequent branch looks like a smaller version of the previous branch, we calculated the projected area using the empirical relationships for branch-projected area valid for mangrove species common in the Pearl River Delta[44]. This gives 2 m^2 for a projected area A without leaves and 6.04 m^2 with leaves. However, this estimate has to be reduced because of branch realignment, which can result in a 50% reduction in the projected area[58]. Thus, we consider a maximum projected frontal surface area per tree of 3 m^2 (with leaves) and 1 m^2 (no leaves) (see description of experiments in Table 1). In the mangrove parameterisation we implemented in FVCOM, the projected area is not constant, it is further reduced considering that in inter-tidal areas, the plants are not always fully submerged. When the water level is less than the height of the plant, which on average for a dense tall mature mangrove forest in the Pearl River Delta we assumed to be 3 m[44], the projected frontal surface area is reduced proportionally to the water level height.

To reproduce Typhoon Hato (2017), we forced the FVCOM Pearl River Delta model with wind velocity and air pressure calculated using the Holland parametric model[59,60], which uses observed maximum wind speed and radius of maximum winds to calculate radial profiles of sea level pressure and winds in a tropical cyclone. Observations were obtained from 3-hourly data provided by the International Best Track Archive for Climate Stewardship (IBTrACS) Version 4. This approach was preferred to the usage of atmospheric model reanalysis, where the peaks in wind velocity (and thus in water levels) can be underestimated[41]. Although the track of Typhoon Hato is along a very typical track followed by tropical cyclones near the Pearl River Delta[61], further research is needed to address how storm properties, such as duration and intensity, or a different storm track, would modulate the attenuation offered by mangroves.

Additionally, we have investigated how the effectiveness of mangroves could change with SLR. We have repeated the high-drag experiments for the 600 m patch in Shenzhen Bay and for the patch from Hualong to Lianhuashan in the upper river channels with an increase in mean sea level imposed at the boundary of the model domain (as done in a previous study[41]). The three future SLR scenarios chosen are 30, 50 and 90 cm (Experiments 11–19 in Table 1). These correspond to the median (50th percentile) and upper limit (95th percentile) by 2050 (30 and 50 cm, respectively) and 90 cm is the median by 2100 of the regional (specific for the Pearl River Delta area) sea level projections[62] for the 'High-end' Representative Concentration Pathway (RCP) 8.5 future climate scenario. However, the model experiments do not necessarily correspond to water levels for a specific climate scenario or time horizon. The applicability of our results is much broader, for example, 30 cm is the RCP 8.5 scenario in 2040 (95th percentile) and 50 cm could equally apply to the RCP 4.5 scenario in 2060 (95th percentile) or in 2090 (50th percentile), while 90 cm is the upper limit in 2100 for the RCP 4.5 scenario[62]. We did not simulate any SLR scenario higher than 1 m. In our model setup, we are simulating a fully protected coastline with mangroves placed in front of a seawall, no extra land can get inundated and no sediment accretion will happen. In this case, the mangroves will be drowned and ineffective with SLR higher than 1 m.

Data availability

The Pearl River Delta FVCOM model experiments presented in this manuscript are available online at https://doi.org/10.5281/zenodo.7414744.

Code availability

The FVCOM model version used to generate the simulations described in this paper can be found in the UK FVCOM Users' code development repository: https://github.com/UK-FVCOM-Usergroup/uk-fvcom.

Received: 5 January 2022; Accepted: 23 December 2022;
Published online: 07 January 2023

References

1. IPCC. *IPCC Special Report on the Ocean and Cryosphere in a Changing Climate* (eds. Pörtner, H.-O. et al.) 755 pp. (Cambridge University Press, Cambridge, UK and New York, NY, USA, 2019). https://doi.org/10.1017/9781009157964.
2. Secretariat, UNFCCC. *Nationally Determined Contributions Under the Paris Agreement: Synthesis Report by the Secretariat* (UN Framework Convention on Climate Change, 2021).
3. Menéndez, P., Losada, I. ñigoJ., Torres-Ortega, S., Narayan, S. & Beck, M. W. The global flood protection benefits of mangroves. *Sci. Rep.* **10**, 1–11 (2020).

4. Bayraktarov, E. et al. The cost and feasibility of marine coastal restoration. *Ecol. Appl.* **26**, 1055–1074 (2016).
5. Bouillon, S. et al. Mangrove production and carbon sinks: a revision of global budget estimates. *Global Biogeochem. Cycles* **22** (2008).
6. Temmerman, S. et al. Ecosystem-based coastal defence in the face of global change. *Nature* **504**, 79–83 (2013).
7. Möller, I. et al. Wave attenuation over coastal salt marshes under storm surge conditions. *Nat. Geoscience* **7**, 727–731 (2014).
8. Mazda, Y., Magi, M., Kogo, M. & Hong, P. N. Mangroves as a coastal protection from waves in the tong king delta, vietnam. *Mangroves and Salt Marshes* **1**, 127–135 (1997).
9. Mazda, Y., Magi, M., Ikeda, Y., Kurokawa, T. & Asano, T. Wave reduction in a mangrove forest dominated by sonneratia sp. *Wetl. Ecol. Manag.* **14**, 365–378 (2006).
10. McIvor, A. L., Möller, I., Spencer, T. & Spalding, M. Reduction of wind and swell waves by mangroves. *Natural Coastal Protection Series: Report 1. Cambridge Coastal Research Unit Working Paper 40.* ISSN 2050–7941 (The Nature Conservancy and Wetlands International, 2012).
11. Horstman, E. M. et al. Wave attenuation in mangroves: a quantitative approach to field observations. *Coast. Eng.* **94**, 47–62 (2014).
12. Maza, M., Lara, J. L. & Losada, I. J. Experimental analysis of wave attenuation and drag forces in a realistic fringe rhizophora mangrove forest. *Adv. Water Resour.* **131**, 103376 (2019).
13. Chang, C.-W., Mori, N., Tsuruta, N., Suzuki, K. & Yanagisawa, H. An experimental study of mangrove-induced resistance on water waves considering the impacts of typical rhizophora roots. *J. Geophys. Res. Oceans* **127**, e2022JC018653 (2022).
14. Leonardi, N. et al. Dynamic interactions between coastal storms and salt marshes: a review. *Geomorphology* **301**, 92–107 (2018).
15. Wamsley, T. V., Cialone, M. A., Smith, J. M., Atkinson, J. H. & Rosati, J. D. The potential of wetlands in reducing storm surge. *Ocean Eng.* **37**, 59–68 (2010).
16. Sheng, Y. P., Lapetina, A. & Ma, G. The reduction of storm surge by vegetation canopies: three-dimensional simulations. *Geophys. Res. Lett.* **39** (2012).
17. Hu, K., Chen, Q. & Wang, H. A numerical study of vegetation impact on reducing storm surge by wetlands in a semi-enclosed estuary. *Coast. Eng.* **95**, 66–76 (2015).
18. Smolders, S., Plancke, Y., Ides, S., Meire, P. & Temmerman, S. Role of intertidal wetlands for tidal and storm tide attenuation along a confined estuary: a model study. *Nat. Hazards Earth Syst. Sci.* **15**, 1659–1675 (2015).
19. Stark, J., Plancke, Y., Ides, S., Meire, P. & Temmerman, S. Coastal flood protection by a combined nature-based and engineering approach: Modeling the effects of marsh geometry and surrounding dikes. *Estuar. Coast. Shelf Sci.* **175**, 34–45 (2016).
20. Lawler, S., Haddad, J. & Ferreira, C. M. Sensitivity considerations and the impact of spatial scaling for storm surge modeling in wetlands of the Mid-Atlantic region. *Ocean Coast. Manage.* **134**, 226–238 (2016).
21. Marsooli, R., Orton, P. M., Georgas, N. & Blumberg, A. F. Three-dimensional hydrodynamic modeling of coastal flood mitigation by wetlands. *Coast. Eng.* **111**, 83–94 (2016).
22. Rezaie, A. M., Loerzel, J. & Ferreira, C. M. Valuing natural habitats for enhancing coastal resilience: Wetlands reduce property damage from storm surge and sea level rise. *PLoS ONE* **15**, e0226275 (2020).
23. Kiesel, J., MacPherson, L. R., Schuerch, M. & Vafeidis, A. T. Can managed realignment buffer extreme surges? The relationship between marsh width, vegetation cover and surge attenuation. *Estuaries Coast.* **45**, 345–362 (2021).
24. Fairchild, T. P. et al. Coastal wetlands mitigate storm flooding and associated costs in estuaries. *Environ. Res. Lett.* **16**, 074034 (2021).
25. Krauss, K. W. et al. Water level observations in mangrove swamps during two hurricanes in florida. *Wetlands* **29**, 142–149 (2009).
26. McIvor, A. L., Spencer, T., Möller, I. & Spalding, M. Storm surge reduction by mangroves. *Natural Coastal Protection Series: Report 2. Cambridge Coastal Research Unit Working Paper 35.* ISSN 2050-7941 (The Nature Conservancy and Wetlands International, 2012).
27. Zhang, K. et al. The role of mangroves in attenuating storm surges. *Estuar. Coast. Shelf Sci.* **102**, 11–23 (2012).
28. Liu, H., Zhang, K., Li, Y. & Xie, L. Numerical study of the sensitivity of mangroves in reducing storm surge and flooding to hurricane characteristics in southern Florida. *Cont. Shelf Res.* **64**, 51–65 (2013).
29. Montgomery, J. M., Bryan, K. R., Horstman, E. M. & Mullarney, J. C. Attenuation of tides and surges by mangroves: Contrasting case studies from New Zealand. *Water* **10**, 1119 (2018).
30. Dasgupta, S., Islam, Md. S., Huq, M., Huque Khan, Z. & Hasib, Md. R. Quantifying the protective capacity of mangroves from storm surges in coastal Bangladesh. *PLoS ONE* **14**, e0214079 (2019).
31. Chen, Q. et al. Improved modeling of the role of mangroves in storm surge attenuation. *Estuar. Coast. Shelf Sci.* **260**, 107515 (2021).
32. Tomiczek, T. et al. Physical model investigation of mid-scale mangrove effects on flow hydrodynamics and pressures and loads in the built environment. *Coast. Eng.* **162**, 103791 (2020).
33. Baird, A. H., Bhalla, R. S., Kerr, A. M., Pelkey, N. W. & Srinivas, V. Do mangroves provide an effective barrier to storm surges? *Proc. Natl Acad. Sci.* **106**, E111–E111 (2009).
34. Hu, Z. et al. Mechanistic modeling of marsh seedling establishment provides a positive outlook for coastal wetland restoration under global climate change. *Geophys. Res. Lett.* **48**, e2021GL095596 (2021).
35. Chan, F. K. S. et al. Urban flood risks and emerging challenges in a Chinese delta: the case of the Pearl River Delta. *Environ. Sci. Policy* **122**, 101–115 (2021).
36. Wang, H. et al. Mangrove loss and gain in a densely populated urban estuary: lessons from the Guangdong-Hong Kong-Macao Greater Bay Area. *Front. Mar. Sci.* **8**, 693450 (2021).
37. Ai, B., Ma, C., Zhao, J. & Zhang, R. The impact of rapid urban expansion on coastal mangroves: a case study in guangdong province, china. *Front. Earth Sci.* **14**, 37–49 (2020).
38. Peng, Y. et al. Virtual increase or latent loss? A reassessment of mangrove populations and their conservation in Guangdong, southern China. *Mar. Pollut. Bull.* **109**, 691–699 (2016).
39. Hallegatte, S., Green, C., Nicholls, R. J. & Corfee-Morlot, J. Future flood losses in major coastal cities. *Nat. Clim. Change* **3**, 802–806 (2013).
40. Li, L. et al. Field survey of Typhoon Hato (2017) and a comparison with storm surge modeling in Macau. *Nat. Hazards Earth Syst. Sci.* **18**, 3167–3178 (2018).
41. De Dominicis, M., Wolf, J., Jevrejeva, S., Zheng, P. & Hu, Z. Future interactions between sea level rise, tides, and storm surges in the world's largest urban area. *Geophys. Res. Lett.* **47**, e2020GL087002 (2020).
42. Morris, R. L., Boxshall, A. & Swearer, S. E. Climate-resilient coasts require diverse defence solutions. *Nat. Clim. Change* **10**, 485–487 (2020).
43. Hu, W. et al. Mapping the potential of mangrove forest restoration based on species distribution models: a case study in China. *Sci. Total Environ.* **748**, 142321 (2020).
44. van Hespen, R. et al. Analysis of coastal storm damage resistance in successional mangrove species. *Limnol. Oceanogr.* **66**, 3221–3236 (2021).
45. Schuerch, M. et al. Future response of global coastal wetlands to sea-level rise. *Nature* **561**, 231–234 (2018).
46. Alongi, D. M. Mangrove forests: resilience, protection from tsunamis, and responses to global climate change. *Estuar. Coast. Shelf Sci.* **76**, 1–13 (2008).
47. Chen, C., Liu, H. & Beardsley, R. C. An unstructured grid, finite-volume, three-dimensional, primitive equations ocean model: application to coastal ocean and estuaries. *J. Atmos. Ocean. Technol.* **20**, 159–186 (2003).
48. Zheng, P. et al. Tide-surge interaction in the Pearl River Estuary: a case study of Typhoon Hato. *Front. Mar. Sci.* **7**, 236 (2020).
49. Wang, T., Khangaonkar, T., Long, W. & Gill, G. Development of a kelp-type structure module in a coastal ocean model to assess the hydrodynamic impact of seawater uranium extraction technology. *J. Mar. Sci. Eng.* **2**, 81–92 (2014).
50. O'Hara Murray, R. & Gallego, A. A modelling study of the tidal stream resource of the Pentland Firth, Scotland. *Renew. Energy* **102**, 326–340 (2017).
51. De Dominicis, M., O'Hara Murray, R. & Wolf, J. Multi-scale ocean response to a large tidal stream turbine array. *Renew. Energy* **114**, 1160–1179 (2017).
52. Carpenter, J. R. et al. Potential impacts of offshore wind farms on North Sea stratification. *PLoS ONE* **11**, e0160830 (2016).
53. Plew, D. R. Shellfish farm-induced changes to tidal circulation in an embayment, and implications for seston depletion. *Aquac. Environ. Interact.* **1**, 201–214 (2011).
54. Struve, J., Falconer, RogerAlexander & Wu, Y. Influence of model mangrove trees on the hydrodynamics in a flume. *Estuar. Coast. Shelf Sci.* **58**, 163–171 (2003).
55. Jimenez, J. A., Lugo, A. E. & Cintron, G. Tree mortality in mangrove forests. *Biotropica* **17**, 177–185 (1985).
56. Krauss, K. W. & Osland, M. J. Tropical cyclones and the organization of mangrove forests: a review. *Ann. Botany* **125**, 213–234 (2020).
57. Eloy, C. Leonardo's rule, self-similarity, and wind-induced stresses in trees. *Phys. Rev. Lett.* **107**, 258101 (2011).
58. Vollsinger, S., Mitchell, S. J., Byrne, K. E., Novak, M. D. & Rudnicki, M. Wind tunnel measurements of crown streamlining and drag relationships for several hardwood species. *Can. J. For. Res.* **35**, 1238–1249 (2005).
59. Holland, G. J. An analytic model of the wind and pressure profiles in hurricanes. *Mon. Weather Rev.* **108**, 1212–1218 (1980).
60. Holland, G. J., Belanger, J. I. & Fritz, A. A revised model for radial profiles of hurricane winds. *Mon. Weather Rev.* **138**, 4393–4401 (2010).

61. Takagi, H., Xiong, Y. & Furukawa, F. Track analysis and storm surge investigation of 2017 Typhoon Hato: were the warning signals issued in Macau and Hong Kong timed appropriately? *Georisk* **12**, 297–307 (2018).
62. Jackson, L. P. & Jevrejeva, S. A probabilistic approach to 21st century regional sea-level projections using RCP and High-end scenarios. *Glob. Planet. Change* **146**, 179–189 (2016).

Acknowledgements

This work is part of the ANCODE (Applying nature-based coastal defence to the world's largest urban area-from science to practice) project, supported by three-way international funding through the Netherlands Organisation for Scientific Research (NWO, lead funder, Grant ALWSD.2016.026), the China's National Natural Science Foundation (NSFC, Grant 51761135022), and the UK Research Councils (UKRI). The UK funding is through the NEWTON fund under the EPSRC Sustainable Deltas Programme, Grant EP/R024537/1. Zhan Hu has been also supported by the NSFC Grant 42176202, the Innovation Group Project of Southern Marine Science and Engineering Guangdong Laboratory (Zhuhai; Grant no. 311021004), the Guangdong Provincial Department of Science and Technology (2019ZT08G090), and the 111 Project (B21018). Peng Zheng was also funded by the NSFC Grant 42006154. The authors thank Peng Yao for the help with the bathymetry data for the FVCOM model and Svetlana Jevrejeva, Ming Li and Marta Payo Payo for all the useful discussions and feedbacks.

Author contributions

M.D.D. and J.W. devised the conceptual idea. M.D.D. conceived, planned and performed the model simulations and analysed the results. R.v.H. contributed to the development of vegetation parameterisation and scenarios. P.Z. developed the FVCOM model implementation for the Pearl River Delta and the South China Sea. J.W. and Z.H. supervised the findings of this work and were responsible for the research activity planning and execution. M.D.D. took the lead in writing the manuscript. All authors discussed the results and contributed to the final manuscript.

Competing interests

The authors declare no competing interests

Additional information

Supplementary information The online version contains supplementary material available at https://doi.org/10.1038/s43247-022-00672-7.

Correspondence and requests for materials should be addressed to Michela De Dominicis or Zhan Hu.

Peer review information *Communications Earth & Environment* thanks Harshinie Karunarathna, Geoff Richards and the other, anonymous, reviewer(s) for their contribution to the peer review of this work. Primary Handling Editors: Adam Switzer and Clare Davis.